Mechanical Consequences of Suffusion on Undrained Behaviour of a Gap-graded Cohesionless Soil - An Experimental Approach

Geotechnical Testing Journal

doi:10.1520/GTJ20160145 / Vol. 40 / No. 6 / November 2017 / available online at www.astm.org

Amirhassan Mehdizadeh,[1] Mahdi M. Disfani,[2] Robert Evans,[1] Arul Arulrajah,[1] and D. E. L. Ong[3]

Mechanical Consequences of Suffusion on Undrained Behaviour of a Gap-Graded Cohesionless Soil - An Experimental Approach

Reference

Mehdizadeh, A., Disfani, M. M., Evans, R., Arulrajah, A., and Ong, D. E. L., "Mechanical Consequences of Suffusion on Undrained Behaviour of a Gap-Graded Cohesionless Soil - An Experimental Approach," *Geotechnical Testing Journal*, Vol. 40, No. 6, 2017, pp. 1026–1042, https://doi.org/10.1520/GTJ20160145. ISSN 0149-6115

ABSTRACT

Fine particles may migrate in the preexisting pores of an internally unstable soil matrix caused by water flow. This migration changes the fine particle distribution and content at different zones and can affect the mechanical properties of these soils. Due to the different roles that fine particles can play in the force chains of an internally unstable soil, the available geometrical assessment methods do not predict post-erosion behavior of the soil. The fine particles may sit loose in the voids, provide lateral support for the primary soil matrix, or participate directly in stress transfer. This will depend on the fine content, particle size distribution, constriction size, relative density, stress path, and particle shape. However, to evaluate the post-erosion behavior accurately, computational modelling or experimental investigation needs to be conducted. A modified triaxial apparatus connected to a water supply system and collection tank was developed to investigate the post-erosion behavior of an internally unstable cohesionless soil under different loading patterns in undrained conditions. This system allowed all test phases to be completed, including erosion inside the triaxial chamber to remove any possible impact of specimen disturbance. The results suggest that the undrained shear strength of the eroded specimen increased at small vertical strains (0–4 %) under monotonic and cyclic loadings, whereas the initial modulus of elasticity remained unchanged. Also, the eroded specimen showed much higher resistance against cyclic loadings, whereas the non-eroded specimen was liquefied during less than five cycles of loading. This improvement was due to a better interlock between coarse particles due to erosion of fine particles. The hardening strain behavior of the non-eroded specimen changed to limited flow deformation due to a decrease in the fine content. The flow deformation of the eroded specimen at medium strain may be due to the local increase in lubrication effect of fine particles in the eroded specimen.

Keywords

erosion-triaxial apparatus, internal erosion, suffusion, internal stability, post-erosion soil behavior

Manuscript received June 30, 2016; accepted for publication May 16, 2017; published online October 11, 2017.

[1] Department of Civil and Construction Engineering, Swinburne University of Technology, John Street, Hawthorn, Victoria 3122 Australia http://orcid.org/0000-0001-7711-8128 (A.M.), http://orcid.org/0000-0003-1998-2537 (R.E.), http://orcid.org/0000-0003-1512-9803 (A.A.)

[2] Department of Infrastructure Engineering, The University of Melbourne, Grattan St, Parkville, Victoria 3010, Australia (Corresponding author), e-mail: mmiri@unimelb.edu.au, http://orcid.org/0000-0002-9231-8598

[3] Department of Civil Engineering, Swinburne University of Technology Sarawak Campus, 93350 Jalan Simpang Tiga, Kuching, Sarawak, Malaysia http://orcid.org/0000-0001-8604-8176

Introduction

For granular soils, if only the coarse particles participate in the primary soil skeleton, the fine particles can migrate through the preexisting pores if the required hydraulic forces are present. The erosion process of these particles is known as suffusion, according to the International Commission on Large Dams (ICOLD) (2015), if no change in soil volume occurs. However, the local and/or general hydraulic conductivity properties of the soil may still change. This is a long-term phenomenon and may occur over a very long period of time. If these eroded particles provide secondary support for the soil load-bearing matrix or contribute partially to the force chains, the soil shear strength may change significantly. In some extreme cases, suffusion may lead to considerable settlements or catastrophic failures in hydraulic structures. A granular soil is vulnerable to suffusion if the fine particles carry no loads or (in some cases) support a small percentage of the effective stresses in comparison with the coarse particles. Gap-graded soils like sandy gravels or silty sands can be classified as geometrically unstable if the fine particles are smaller than the pore sizes.

Terzaghi (1925) was one of the first researchers to suggest that effective stresses decrease due to hydraulic stresses in the upward flow in sands and, if the hydraulic gradient reaches a critical magnitude, particles will dislodge from the soil body. This process is defined as hydraulic heave in sandy materials. Subsequently, researchers like Skempton and Brogan (1994), Li and Fannin (2011), Shire et al. (2014), and Moffat and Herrera (2014) attempted to expand Terzaghi's theory further for gap-graded soils. They showed that the required hydraulic gradient to move the finer particles is much lower than the critical hydraulic gradient presented by Terzaghi, especially if these fine particles do not fully contribute in the primary soil matrix.

Experimental investigation can be divided into two main parts. Some researchers used rigid-wall permeameter cells to investigate the initiation of internal instability and effective parameters that accelerate the process (Kenney et al. 1985; Skempton and Brogan 1994; Moffat and Fannin 2006; Sail et al. 2011; Indraratna et al. (2015). Some others like Chang and Zhang (2011), Xiao and Shwiyhat (2012), and Ke and Takahashi (2014a) have focused on the post-erosion response of cohesionless soils. For instance, a new experimental device was developed by Bendahmane et al. (2008) based on an ordinary triaxial apparatus for evaluating initiation of internal erosion in sandy clay samples. Test results indicated that erosion of clay particles started first and this was classified as suffusion. However, there was a second threshold in the hydraulic gradient above which erosion of sand particles initiated. This led to backward erosion and finally collapse of the whole sample. It was understood that suffusion and backward erosion both were affected by initial clay content. Ahlinhan and Achmus (2010) investigated the effects of flow direction and relative density on the erosion process of different soil gradations. This study suggested that an immediate increase in the flow velocity is a consequence of the onset of erosion. However, this increase is more obvious for internally unstable soils. Moffat and Fannin (2011) investigated the influence of the onset of instability on the local hydraulic gradient and presented a hydromechanical envelope in effective stress-critical hydraulic gradient space governing internal stability of cohesionless soils. This envelope appears to be independent of the flow direction, and internal instability may be triggered either by an increase in hydraulic gradient or a decrease in effective stress. Moffat et al. (2011) performed permeameter tests on widely graded cohesionless soils to investigate the influence of internal erosion. These experiments showed that suffusion is a time-dependent phenomenon and causes soil particle migration with no change in volume of the specimen. Suffusion can be classified as the next phase of suffusion when volumetric strains occur due to the washing out of particles.

Although different aspects of erosion initiation have been studied extensively, the effect of suffusion on mechanical soil properties is a new research area. One of the first studies to evaluate the post-erosion behavior of cohesionless soil was conducted by Ke and Takahashi (2012), in which the variation of soil strength was measured using a miniature cone penetration test. They found a reduction in the cone tip resistance after internal erosion was attributed to the loss of fine particles. The variation of drained shear strength due to internal erosion was investigated for the first time by Chang and Zhang (2011). They performed drained triaxial tests (pre- and post-erosion) under different consolidation stress paths. The results showed that the peak shear strength decreased significantly and the stress-strain behavior changed from dilative to contractive due to the removal of a certain amount of fine particles and an increase in void ratio. Xiao and Shwiyhat (2012) performed post-suffusion undrained triaxial compression testing on gap-graded specimens. Higher undrained shear strength was observed for the eroded specimens. They suggested that this might have been due to the loss of saturation during the erosion phase as the bottoms of the samples were subjected to atmospheric pressure. Ke and Takahashi (2014a) studied the drained and undrained behavior of gap-graded sand under monotonic and cyclic loadings. This revealed that the post-erosion drained and undrained compressive strength decreased and increased, respectively.

In other research works conducted by Ke and Takahashi (2014b, 2015), the mechanical consequences of suffusion were investigated with different initial fine contents and confining pressures. Whereas specimens with 35 % fine content showed completely contractive drained behavior, the volumetric strain behavior of specimens with 15 % to 25 % fine content was initially contractive but then changed to dilative at the medium strain range. In addition, the drop in the drained shear strength after

suffusion was more obvious for the specimen with 35 % fine content.

In comparing the results of these studies, it is evident that the consequences of erosion on the mechanical soil properties and behavior of cohesionless soils are not well understood and some conflict exists. In addition, previous experimental attempts have had their own technical issues. For instance, the saturation percentage of the specimens was 85 % in studies conducted by Chang and Zhang (2011) and Xiao and Shwiyhat (2012), which resulted in some errors. Xiao and Shwiyhat (2012) mentioned that the bottom mesh they used may not have been selected accurately with respect to the size of the erodible particles. Ke and Takahashi (2014a, 2014b) solved the problem of losing saturation. However, the rotary pump they used in the test produced a jet flow on the soil specimen at the beginning of each erosion stage, which affected specimen deformation (radial and volumetric strains were measured via using local strain gauges). It is plausible that local instruments had a reinforcing influence on the sample and may have caused considerable error in the measurement of strain and soil behavior.

Computational investigation of internal erosion has been attracting more interest from the last decade. However, in comparison to the laboratory research, there are still many conceptual ambiguities that need to be clarified. For instance, Wood et al. (2010) used two-dimensional discrete element modelling to investigate the mechanical consequences of erosion by the software package PFC-2D. Instead of considering a coupled flow and particle removal, the process of erosion was modelled by progressively removing the fine particles, whereas the external stresses were kept constant. This numerical modelling showed that the particle removal increased the specific volume ($v = 1 + e$), which led to volumetric compression due to more open internal structure, narrowed the soil grading, and raised the critical state line. The consequence of this process was a lower available strength and occurrence of distortional strains. Although this research provided a better understanding of consequences of particle removal, no evidence provided showed the validity of the model. They believed that internal erosion is a time-dependent phenomenon and changes the actual fabric of the material, and it cannot be simulated only by mixing up particles with different sizes and randomly removing the small particles. In other research, a multi-scale approach including a discrete element model and an analytical micromechanical model was proposed by Scholtès et al. (2010) and Hicher (2013) to assess internal erosion effects on the mechanical properties of a granular medium and induced deformations during the erosion process. It was found that removal of particles at shear stress ratios lower than 0.72 resulted in contractive deformations and samples reached a new stable state. However, instability and dilation were observed when particle extraction occurred at shear stress ratio greater than 0.72. This threshold value for shear stress ratio was related to the residual state at large shear deformation, which is known as the critical state. This meant that under a shear stress state lower than the critical one, particle rearrangement acted as a self-healing factor to counterbalance the effects of particle erosion. In addition, regardless of percentage of the particle removal, this is the mobilized friction that controlled the failure of assembly. Moreover, it was found that due to increase in the initial porosity, the specimen behavior changed from dilative to contractive, and a drop in the shear strength was observed. In fact, particle removal decreased the internal friction angle and weakened the assembly. They concluded that the mechanical response in terms of internal friction, volumetric strain, and residual sate were independent of the initial stress state under which erosion was conducted.

This paper has attempted to solve some of these previously observed issues in the post-erosion experimental investigation. To achieve this, a triaxial chamber was modified to perform suffusion tests inside the triaxial cell, which also involved the development of the water supply and collection system. This system proved to be versatile, which allowed three different sized specimens with diameters of 50, 75, and 100 mm to be tested. This paper also explains the design principles and presents the performance of the apparatus during each different stage of testing. Preliminary test results are also discussed in terms of stress-strain behavior (measured using photogrammetry techniques) of the eroded and non-eroded specimens under monotonic and cyclic loadings.

Testing Apparatus

To investigate the post-erosion behavior of internally unstable soils, the soil specimen first needs to be exposed to water flow to initiate erosion. Then, the triaxial test is performed to evaluate soil response. Due to the granular nature of the material and to avoid any disturbance, a triaxial chamber was modified to perform saturation, consolidation, erosion, and shearing successively without removing the specimen. For this reason, the top cap and base plate of a triaixal chamber were modified in order to apply the hydraulic gradient and allow the soil particles to be eroded and washed out of the chamber. The water supply system was designed to provide a range of water heads or flow rates. The fabricated collection system can measure the weight of the eroded particles continuously during the test. This system allows for studying pre- and post-suffusion soil behavior under different stress paths and loading patterns.

The water supply system was designed to maintain a constant flow condition (i.e., flow rate) over a long period of time. Richards and Reddy (2008) stated that if Darcy's Law is applicable during the soil seepage, a decrease in hydraulic conductivity leads to an increase in hydraulic gradient at a constant flow rate. Due to this coupling effect, they suggested that considering only the critical hydraulic gradient may not be correct for cohesionless type soils. Therefore, a flow controller was connected to the pipe between

FIG. 1 Water supply system.

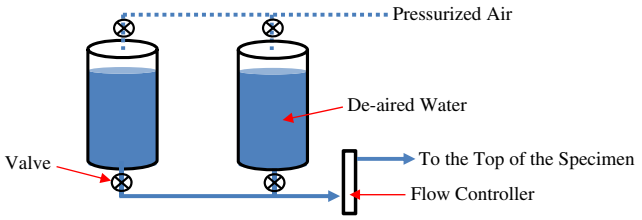

the water supply system and erosion cell to control the flow rate. In addition, two pressure transducers were installed at the top and bottom of the specimen for direct measurement of the general hydraulic gradient across the full height of the sample. The water supply unit was composed of two water tanks (connected to each other in parallel), a flow controller, and an air pressure supply. These cells were filled with de-aired water, whereas the air pressure was applied to the top of the water inside the cell. Continuous water supply was provided using an exclusive outlet and supply valve to each cell. **Fig. 1** illustrates the water supply system.

To apply different water heads and flow rates, a flow controller with a maximum operating pressure and temperature of 1,370 kPa and 93°C was connected to the outlet pipe of the cells. This allowed a flow rate up to 500 mL/min to be applied to the top of the sample.

For erosion tests to be performed in the triaxial chamber, a new top cap, bottom plate, and base plate were manufactured. The top cap consisted of a hollow cap with a 5-mm-thick perforated steel plate with a 2-mm opening size. To diffuse the water on the sample contact interface uniformly and reduce the jet flow reported by Ke and Takahashi (2014b), the top cap was filled with glass spheres of various sizes (**Fig. 2**). To avoid particle migration to the top cap during the saturation process, a mesh with an aperture smaller than the smallest particle size (0.075 mm) was placed between the top of the specimen and top plate.

The original base plate was replaced with a 10-mm-thick netted plate, a funnel shaped pedestal, and a new base plate with a conical trough to provide enough space for the eroded particles to move into the collection chamber without clogging. A rigid mesh was placed on the netted plate to hold the coarse fraction (soil body) and let the fine particles (erodible particles) out. The mesh size was determined based on the smallest particle size in coarse fraction or constriction size. For the tests reported in this paper, a 1.18-mm mesh was used. **Fig. 3** shows the various parts of the modified base cell. Because the pedestal is detachable, it is practical to test specimens with different dimensions. Solid plates were also manufactured for performing ordinary triaxal tests to compare pre- and post-erosion soil behavior and reduce the mechanical errors (**Fig. 3d**). Although, different end restraints may be created due to the use of dissimilar bottom plates, initial ordinary tests did not show any significant variation in results between specimens sitting

FIG. 2 Top cap filled with glass spheres.

on different plates. In addition, a new pedestal was designed and fabricated to allow water to discharge and the erosion of particles from the bottom of the cell while maintaining the load (**Fig. 4**).

The collection system was designed to collect the eroded particles and discharged water from the cell, as well as to simultaneously measure the weight of the eroded particles and maintain a constant back pressure to keep the specimen's base saturated. The main design challenge was to continuously measure the weight of the dislodged particles without losing the back-pressure while eliminating the influence of the inlet flow. To overcome these limitations, Ke and Takahashi (2014a) came up with a practical solution. The measuring tray was submerged and a stable water level was maintained. To eliminate the effect of water weight, the measuring tray was connected to a submersible load cell (10 g resolution) and suspended inside a poly (methyl methacrylate) cell (inner cell) full of water. The water level at the top of this cell was kept constant and the inlet flow from the triaxial chamber was discharged from the inner cell into the main chamber via drainage holes in the wall of the inner cell. To reduce the flow jet effect reported by Ke and Takahashi (2014a) and related noise with the load cell readings, a plastic funnel was placed in the inner cell. The collected water in the main chamber was discharged at specific intervals. The air above the water was pressurized/equalized to the back-pressure applied to the specimen during the test (**Fig. 5**).

Strain Measurement

In conventional triaxial testing, the measured vertical strain at the top of the sample is the average of the vertical strains, which is inaccurate. In addition, global deformation measurement cannot detect local failures and strains. There are different types of local

FIG. 3

Details of modified cell base: (a) base plate, (b) funnel-shaped pedestal, (c) netted plate, and (d) solid plate to perform ordinary triaxial tests.

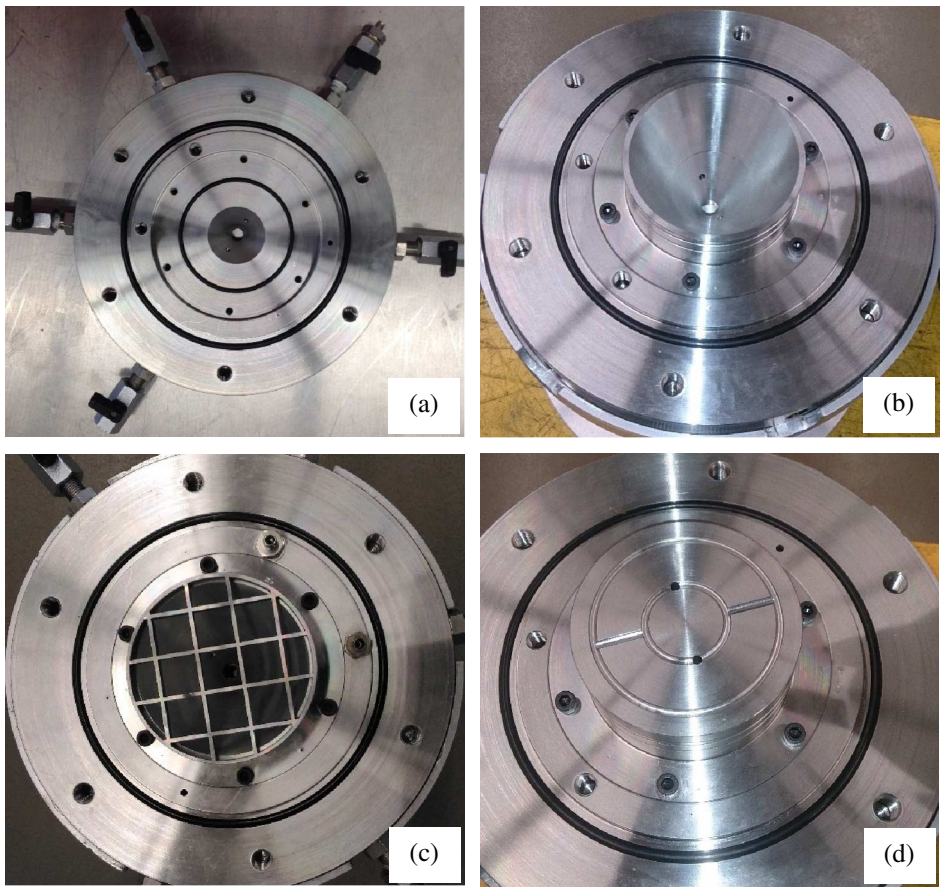

FIG. 4

New pedestal to apply axial force to the specimen; (a) top view and (b) bottom view.

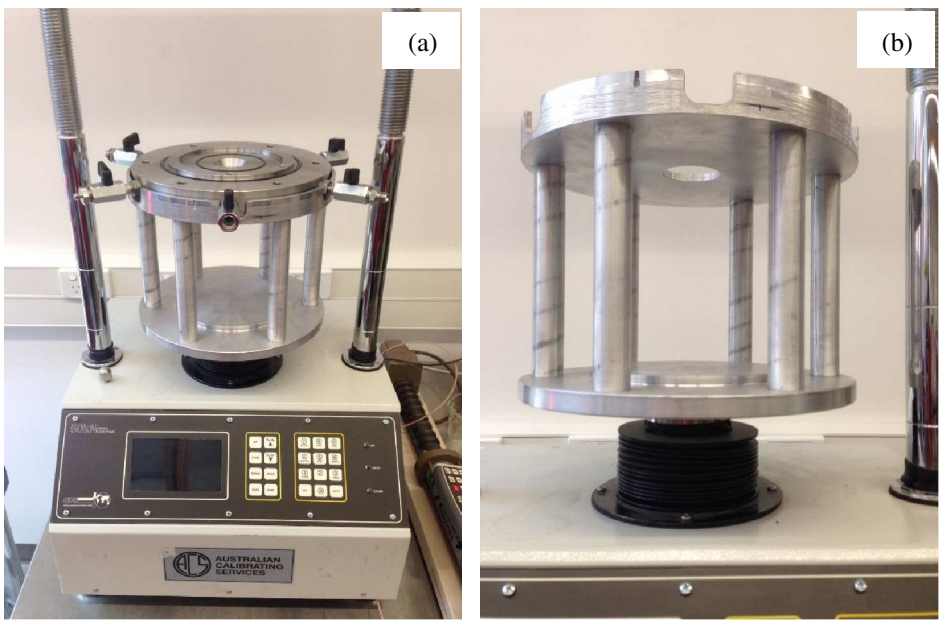

FIG. 5
Collection system details.

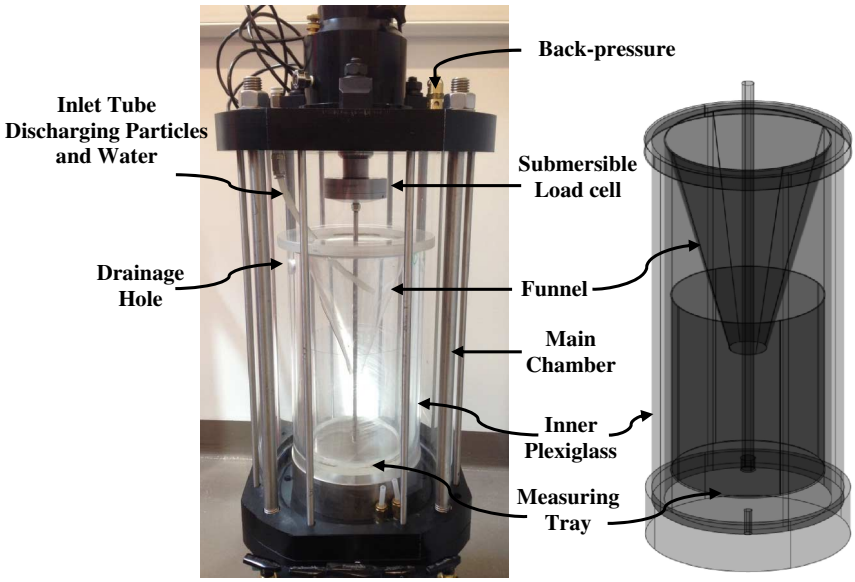

strain gauges that can be connected to the body of the sample. However, these instruments apply a confining and reinforcing pressure on the soil sample that may affect the soil response during shearing. To reduce these errors, photogrammetry techniques were employed to measure the local vertical and horizontal strains during the test.

Volumetric strains are usually measured by pore water variations in the triaxial testing. However, due to the discharge of water during the erosion stage, it is not possible to use this method. Cell water variation measurement is another method, but some considerations must be taken into account. The volume of the cell may be affected by cell pressure, variation in room temperature, creep of material, unloading/reloading, and the movement of loading piston inside the cell. Therefore, significant calibrations are required before testing, which is a disadvantage. Because the conventional measurement of deformation at the top of the specimen and measurement of the specimen volume change by monitoring the cell volume brings about many errors and disadvantages, the technique of photogrammetry was employed to measure the volumetric strains and the vertical and lateral strains during erosion and undrained shearing. Uchaipichat et al. (2011) and Mehdizadeh et al. (2015) have explained the details of volumetric and local strains measurement using photogrammetry and related challenges.

Testing Material and Sample Preparation

Natural sand with the gradation curve shown in **Fig. 6a** was used for this research. To assure the tested specimen was internally unstable, a gap-graded specimen was created by manually removing particle sizes between 0.3 to 1.18 mm and 2.36 to 10 mm. The gap-graded specimens with 25 % fine content were prepared using particles sizes of 0.075–0.3 mm (fine fraction) and 1.18–2.36 mm (coarse fraction) (**Fig. 6b**). **Table 1** presents the physical properties of the mixture.

Constriction size was calculated to be 0.28 and 0.3 mm using Kenney et al. (1985), Indraratna et al. (2007), and Dallo et al. (2013) equations. For this specimen, this suggests that the whole fine particles (≤0.3 mm) can be eroded if the hydraulic and stress-state conditions are met.

Fraser (1935) stated that particle shape affects hydraulic conductivity by varying the size and shape of the pores and the packing level. Permeability increases as true sphericity is decreased, which was also later confirmed by Guimaraes (2002). In other research studies conducted by Marot et al. (2012) and Fleshman and Rice (2014), it was found that angularity of particles improved the erosion resistance. These studies showed the importance of the particle shape in the internal erosion study. To take into account the influence of particle shape in the test result justification, images of the particle shape were captured using a digital microscope with USB (Universal Service Bus) output (**Fig. 7**) and the images were analyzed by ImageJ software package. Particle shape characteristics including circularity, roundness, and aspect ratios were measured based on the definitions suggested by Ferreira and Rasband (2012) (**Table 2**). **Table 2** indicates that coarse particles are more angular than fine particles, as circularity of coarse fraction, especially for particles in the range of 1.7–2.36 mm, is significantly lower than fine particles. This can also be noticed by a drop in aspect ratio.

Internal stability of the prepared mixture was assessed based on the available methods to ensure that suffusion would occur

FIG. 6 Particle size distribution for (a) original soil and (b) tested soil.

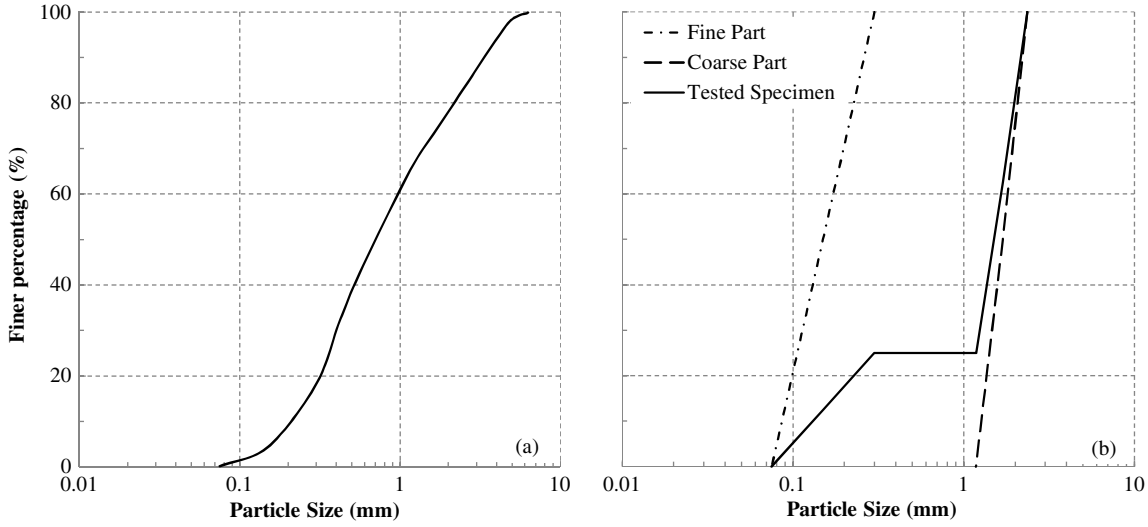

during the erosion stage (**Table 3**). It can be seen that out of twelve methods, eight suggested that the mixture was internally unstable and suffusion would occur if the hydraulic gradient was high enough.

It is critical to perform erosion tests on completely uniform specimens in terms of density, particle size distribution, and void ratio. Otherwise, the test results may show considerable discrepancies, even under similar stress paths and hydraulic gradients. Different methods are available to prepare uniform specimens for triaxial testing, such as the under-compaction or moist tamping method (Ladd 1978; Frost and Park, 2003; Jiang et al., 2003; Bradshaw and Baxter 2007) and the slurry method (Kuerbis and Vaid 1988; Carraro and Prezzi 2008). For this research, the under-compaction moist tamping technique presented by Ladd (1978) with modifications employed by Jiang et al. (2003) was used to prevent segregation during sample preparation and create specimens with maximum uniformity across the specimen height. Following this method, a specimen with 75 mm in diameter and 150 mm in height was reconstituted in 10 layers.

TABLE 1. Physical properties of tested soil.

Physical Property	Value	Physical Property	Value
Specific Gravity, G_s	2.645	$D_{c35(densest)}$[d]	0.226
Maximum void ratio, e_{max}	0.671	$D_{c35(loosest)}$[e]	0.702
Minimum void ratio, e_{min}	0.36	D_{c35}[f]	0.292
Initial relative density, D_r (%)	60	Uniformity coefficient, C_u	12.14
Moisture content, w (%)	6	Curvature coefficient, C_c	7.1
Fine Content, FC (%)	25	$(H/F)_{min}$[g]	0.08
Porosity, n	0.32	(D'_{15}/d'_{85})[h]	5.2
D_{up}/D_{bt}[a]	3.93	Gap ratio, G_r[i]	3.93
D_{erod}, (mm)[b]	0.103	$h' = D_{90}/D_{60}$	1.29
D^*, (mm)[c]	0.28–0.3	$h'' = D_{90}/D_{15}$	12.8

[a]D_{up} and D_{bt} are maximum and minimum sizes in the gap zone.
[b]Maximum erodible particle size (Burenkova 1993).
[c]Constriction size (Kenney et al. 1985).
[d]Controlling constriction size for the densest state (Dallo et al., 2013).
[e]Controlling constriction size for the loosest state.
[f]Constriction size (Indraratna et al., 2007).
[g]F is the passed fraction by weight finer than d, and H is the weight fraction between d and $4d$ (Kenney and Lau 1985, 1986).
[h]D'_{15} is the particle diameter in which 15 % by weight of coarser particles passed, and d'_{85} is the particle diameter in which 85 % by weight of fine particles passed.
[i]$Gr = D_{max}/D_{min}$ of the flat zone (gap zone).

Testing Procedures

To investigate the effect of suffusion on soil behavior under monotonic and cyclic loading, a series of triaxial erosion tests were performed. These tests were performed in five stages: (i) saturation, (ii) consolidation, (iii) erosion, (iv) undrained monotonic shearing or undrained cyclic loading followed by monotonic shearing, and (v) post-erosion particle size distribution (PEPSD). A parallel series of non-eroded specimens were also tested under the same stress paths as a comparison. The details of each stage are explained in the following sections.

The sample was prepared in an internal split mold. To prevent collapse or disturbance of the sample during preparation, a

TABLE 2. Particle shape characteristics.

Particle Size (mm)	Roundness	Circularity	Aspect Ratio
0.075–0.15	0.827	0.874	1.219
0.15–0.3	0.755	0.788	1.23
1.18–1.7	0.815	0.738	1.24
1.7–2.36	0.736	0.707	1.383

TABLE 3. Internal stability evaluation of mixture.

Method	Stability	Method	Stability
U.S. Army Corps of Engineers (1953)	Stable	Kwang (1990)	S (Marginal)
Istomina (1957)	S	Burenkova (1993)	U
Kezdi (1969)	Unstable	Mao (2005)	U
Sherard (1979)	U	Dallo et al. (2013)	U
Kenney and Lau (1985)	U	Chang and Zhang (2013)	S
Kenney and Lau (1986)	U	Moraci et al. (2014)	U

vacuum pressure of 10 kPa was applied. When the triaxial chamber was assembled, the suction was gradually removed, whereas the cell pressure incrementally increased to 10 kPa. Next, to assure a high level of saturation was achieved in a timely manner, carbon dioxide was injected at the bottom of the specimen for two hours. The rate of injection was kept low (1 L/min) to avoid any specimen disturbance caused by gas flow. The cell and back pressure were then linearly and gradually (1 kPa/min) increased to reach 400 and 390 kPa, respectively. These pressures were held for a further 100 minutes to ensure that the specimen was fully saturated. The B-value was also checked at the end of this stage and was recorded to be higher than 93 % for all tested specimens.

Frost and Park (2003) showed that during sample preparation by the moist tamping method, specimens may experience vertical peak stresses of 95–184 kPa for relative densities of 50–75 %. These significant stresses may affect soil behavior and accelerate the development of a shear band. In addition, the magnitude of the applied stress during the moist tamping cannot usually be monitored. This uncertainty may result in a reduction in accuracy, especially in erosion tests that uniformity in dry density and void ratio across the specimen height is necessary. To reduce the effect of the moist tamping stresses, it was decided to consolidate all tests to 150 kPa. Thus, the isotropic consolidation was performed by gradually increasing the cell pressure up to 540 kPa (150 kPa consolidation pressure). The rate of increase was similar to the saturation stage to avoid any disturbance or segregation.

For the eroded tests, the erosion of the specimen was performed after consolidation. Under constant stress condition, de-aired water was allowed to seep downward from the top of the specimen. After each increment, the flow rate was kept constant for one minute to stabilize the seepage flow. The flow rate increased gradually up to 408 mL/min (≈ 92 mm/min for a specimen with 75-mm diameter) and was kept constant for two hours for all tests. This flow rate was higher than the critical flow rate initiates suffusion but lower than the failure flow rate. The failure

FIG. 7

Particles shape: (a) D: 0.075–0.15 mm, (b) D: 0.15–0.3 mm, (c) D: 1.18–1.7 mm, and (d) D: 1.7–2.36 mm.

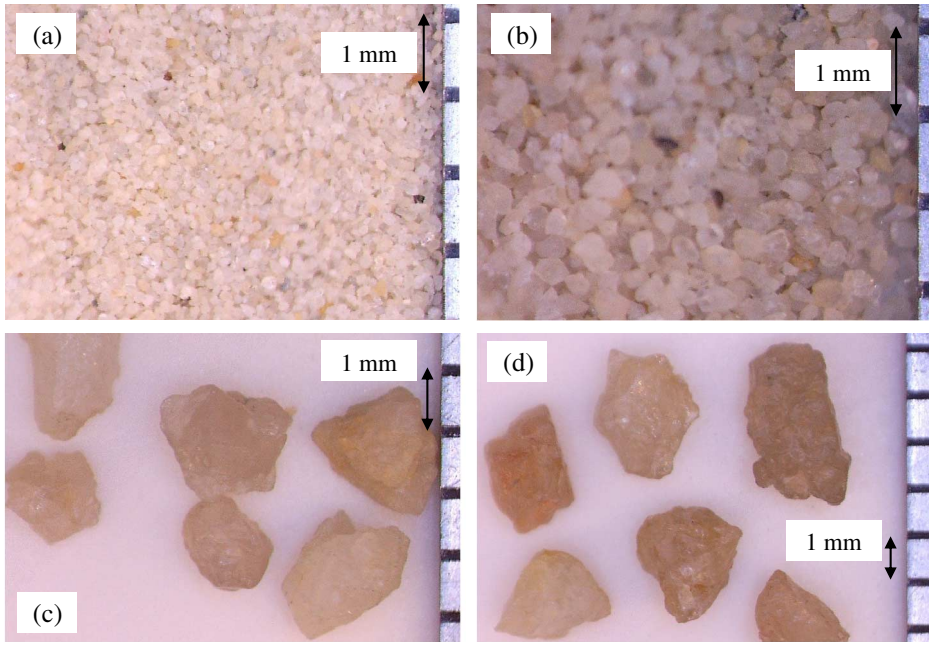

flow rate is defined as a seepage flow rate that causes loss of excessive amounts of particles and causes the soil to experience shear failure due to large seepage forces (Chang and Zhang 2013). It is generally accepted that the critical hydraulic gradient is much lower than one for internally unstable soils. Erosion of fine particles confirmed that the chosen flow rate was higher than the critical value. The maximum applicable flow rate by the flow controller was 500 mL/min. A large flow rate of 408 mL/min (lower than the maximum value) was selected for this experiment to terminate the erosion phase in a reasonable period of time. However, it was applied in a pilot test first to examine whether a global failure occurs in the soil specimen or not. As this did not happen and the soil structure was robust until the end of the erosion phase, this flow rate was chosen for the experiment. The applied flow velocity was equal to 92 mm/min considering the specimen area of 4,418 mm^2. The soil specimen with 75-mm diameter did not fail even under a flow rate of 500 mL/min. To find the failure flow velocity, a soil specimen with 50-mm diameter was prepared under the same condition and subjected to an inflow velocity of 208 mm/min (flow rate of 408 mL/min), which was approximately 2.3 times greater than what was experienced by the soil specimen with 75-mm diameter. The test result showed that this specimen was still stable at the end of the erosion phase, although it experienced larger deformations. These trial and errors indicated that the failure flow rate is not reachable for soil specimens with 60 % relative density and under 150 kPa consolidation pressure due to limitation of the flow controller.

Luo et al. (2013) performed some short-term and long-term suffusion tests. The results indicated that for the long-term tests, the failure hydraulic gradient was much lower than for the short-term tests. They also stated that a long-term large hydraulic gradient may decrease the failure hydraulic gradient significantly. This means that although the adopted flow rate of 408 mL/min was lower than the failure hydraulic gradient, it may cause general collapse of the specimen if the erosion continues for a long time. Therefore, it was decided to terminate the erosion stage after a specific time in all tests by gradually decreasing the inflow. Because two pressure transducers were connected to the top and bottom of the specimen, the general hydraulic gradient and hydraulic conductivity through the specimen length could be measured. When the pore water pressure became stable at the top and bottom of the specimen, the next stage commenced.

Before undrained monotonic or cyclic shearing of the specimen, the B-value was checked again to ensure that the specimen was still fully saturated and above 93 %. It is worth mentioning that no considerable eroded particles were observed during triaxial tests without an erosion stage. It means that the amount of dislodged particles was minor during the saturation and consolidation phases.

Next, post-erosion behavior investigation under undrained monotonic or cyclic loadings was conducted. The initial tests on the non-eroded specimens showed that the excess pore water pressure (EPWP) reached 150 kPa and the liquefaction happened during the first five loading cycles. The cyclic behavior of the samples was investigated under a cyclic stress ratio equal to 0.167 and a period of 120 seconds (equivalent frequency of 0.0083 Hz). Strain-control monotonic shearing was performed at the end of both non-eroded and eroded tests. To allow the pore pressure to reach equilibrium, the vertical strain rate equal to 0.26 %/min (0.385 mm/min) was selected for all specimens.

Experiment Results and Discussion

The primary results of pre- and post-suffusion behavior of an internally unstable soil for various types of loading are presented. Test results in terms of stress-strain behavior, induced EPWP, and stress path during cyclic loading and monotonic shearing are discussed and presented.

The tested specimens in this paper all consist of 25 % fine content, which indicates that the specimen is in the transitional zone suggested by Shire et al. (2014). Consequently, the fine particles may sit loose in the voids or have a considerable role in providing lateral support to the coarse particles or directly contribute in the soil primary fabric. Therefore, experimental investigation is required to predict the post-suffusion behavior of this specimen.

Fig. 8 presents the percentage of the eroded fine particles, vertical and volumetric strains during erosion versus inflow velocity. The residual fine content of the specimens was approximately 10 % after two hours suffusion, which means 66 % of the total available fine particles were eroded during erosion (**Fig. 8a**). It can be seen that the rate of particle erosion increased after reaching the maximum inflow velocity (at 1,380 seconds) and started to decrease after approximately 1,200 seconds and then became stable for the last 1,000 seconds. Vertical and volumetric strains measured by photogrammetry during the erosion stage are shown in **Fig. 8b** and **8c**. As this measurement is based on surface deformations, it cannot be used for the void ratio calculation. **Fig. 8b** shows a jumping pattern in vertical strains like what was observed by Ke and Takahashi (2014a). These discrete spikes were attributed to the local particle rearrangement. Erosion of fine particles that provided a lateral support for the soil stress matrix formed local metastable structures (force chains). This local particle rearrangement helped the soil skeleton to reach a new stable state. **Fig. 8c** indicates volumetric strains during the erosion stage. The soil specimen showed the contractive behaviour and the specimen volume decreased by 2.75 % due to the particles erosion.

The undrained responses of the non-eroded and eroded specimens under monotonic loading (shearing) are illustrated in **Fig. 9**. Under monotonic loading, the non-eroded specimen showed hardening behavior, whereas the eroded specimen showed limited flow deformation. The initial modulus of elasticity

FIG. 8 Variation of (a) eroded fine particles percentage, (b) vertical strains, and (c) volumetric strains during erosion stage versus inflow velocity.

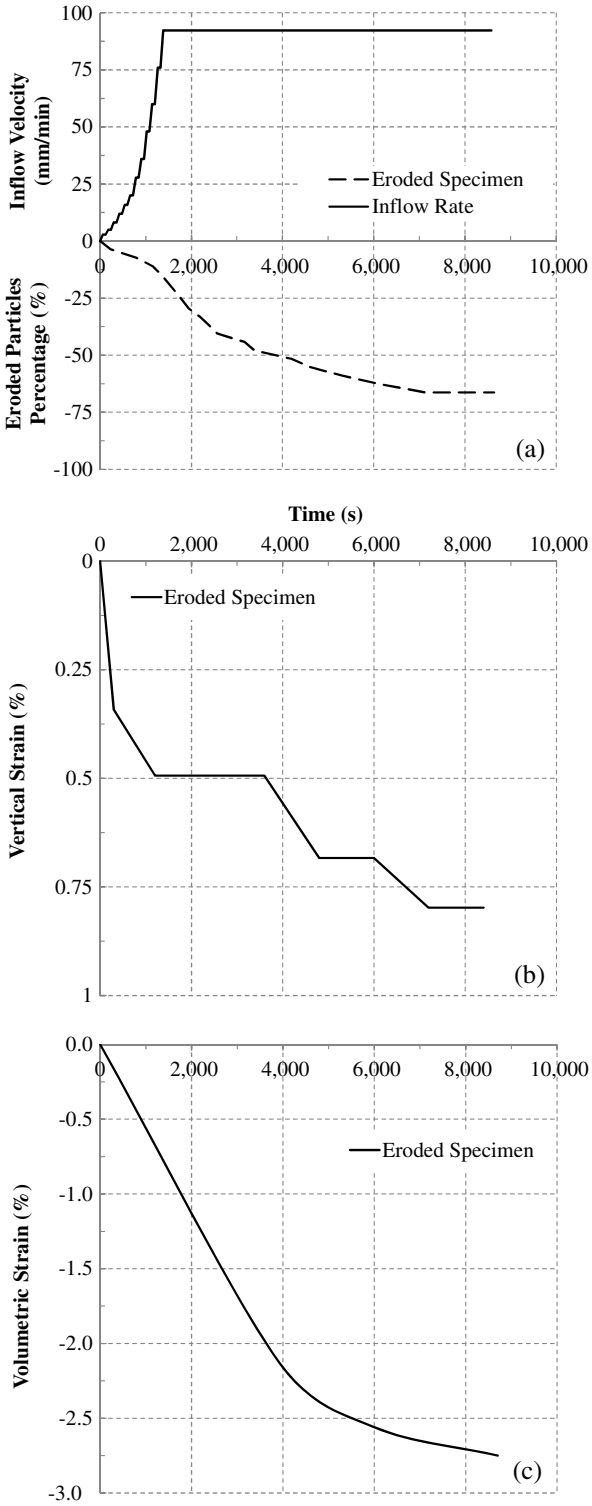

FIG. 9 Pre- and post-suffusion response under monotonic loading: (a) stress-strain behavior, (b) induced EPWP, and (c) stress path.

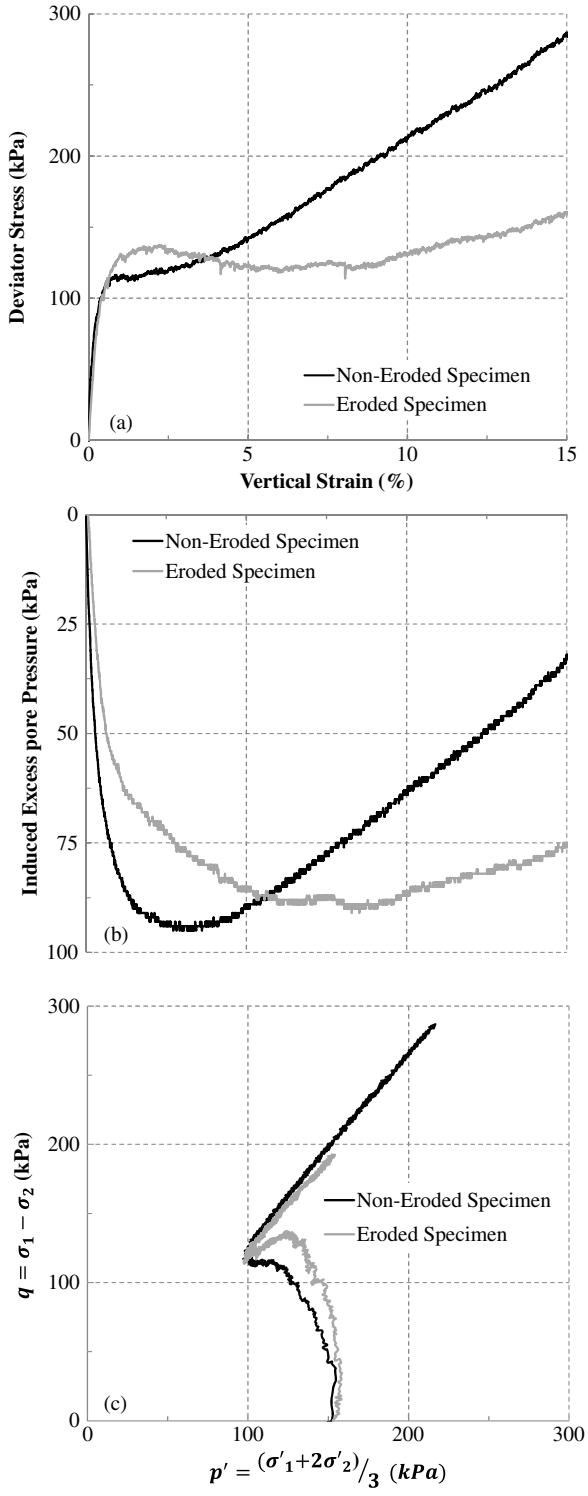

was similar for both specimens. However, the eroded specimen became softer during medium vertical strains. The shear strength of the eroded specimen was greater than the non-eroded specimen for vertical strains less than 4 %. The shear strength then decreased during the next 4 % vertical strain ($3.7 \leq \varepsilon_v \leq 8.4$ %). Finally, the strain hardening behavior was observed at

TABLE 4. Variation of normalized initial peak shear strength and global and intergranular void ratios during erosion stage.

Parameter	Pre-Erosion	Post-Erosion
Normalized Peak Shear Strength	0.39	0.45
Global Void Ratio	0.46	0.67
Intergranular Void Ratio	0.95	0.86

the larger strains until the end of the test, similar for the non-eroded specimen, although the final shear strength was well below the measured value for the non-eroded specimen (**Fig. 9a**). This finding is in agreement with what was reported by Ouyang and Takahashi (2015) for soil specimens with 25 % initial fine content. However, Ke and Takahashi (2015) and Ouyang and Takahashi (2015) observed larger initial secant stiffness for the eroded specimen at very small strains (less than 1 %). They believed that this occurred due to a distinguished packing of soil grains after erosion (accumulation of the fine particles at the spots where the constriction size is smaller than the erodible particles and participation of these clogged particles in force chains). Development of EPWP is shown in **Fig. 9b**. The positive excess pore pressure developed rapidly at the small strains in the non-eroded specimen, whereas it took much longer for the eroded specimen to reach the peak excess pore pressure (8 % vertical strain). However, the maximum values were similar. Another difference between the original and eroded specimen was tendency to dilation. The dilative behavior was observed after reaching 3 and 8 % vertical strain for the original and eroded specimens, respectively (**Fig. 9b**). In addition, it is evident that regardless of erosion of the fine particles, the stresses path eventually ended up on the same transformation state (location of behavioral change from contractive to dilative) and steady state line for both specimens (similar critical friction angle) (**Fig. 9c**). This is also in agreement with Ouyang and Takahashi's (2015) findings.

The initial peak shear strength (S_p was first presented by Ishihara (1993). This point is the beginning of the instability for soils with softening behaviour. **Table 4** shows variation of the normalized initial peak shear strength with the mean effective stress and global and intergranular void ratios pre and post erosion. The normalized value for the peak shear strength is used to eliminate possible effects of stress dependency. It can be seen that the normalized initial peak shear strength improved as erosion progressed despite an increase in the global void ratio after suffusion. However, the intergranular void ratio showed a decrease due to erosion of fine particles. The intergranular void ratio was defined by Mitchell (1993) to consider the contribution of fine particles to the soil stress matrix Eq 1.

$$e_g = \frac{e + FC}{1 - FC} \tag{1}$$

where e_g is the intergranular void ratio, e is the global void ratio, and FC is the fine content in decimal.

The observed drop in the intergranular void ratio was related to the particle rearrangement. Theoretically, a decrease in volume of the fines due to suffusion is added to the real voids, and the final result is that the intergranular void ratio is unchanged. However, if the soil skeleton formed by the coarse particles deforms or settles due to the particle rearrangemeent, the available spaces between the coarse particles may decrease, which could lead to a reduction in the intergranular void ratio.

It was shown in **Fig. 7** and **Table 2** that coarse particles in range of 1.7 to 2.36 mm were more angular in comparison to other particles. Erosion of fine particles might have improved interlocking between coarse particles. This could be the reason of the greater shear strength of the eroded specimen at small strains. However, the flow deformation during the medium vertical strains may have been related to the local concentration of fine particles somewhere in the specimen (probably in the bottom half) or the larger global void ratio of the eroded specimen. This accumulation of the fine particles increased the lubrication locally between coarse particles and led to a steady state until the additional shearing improved the interlocking of the coarse particles in other zones and activated the dilatancy.

Vertical and horizontal local strains during the undrained shearing stage were measured using a photogrammetry technique. As only one camera was used for the photogrammetry, it was necessary to assume that axisymetric volume changes occurred during erosion, which is not completely correct. However, this error can be eliminated by using two prependicular cameras as explained by Uchaipichat et al. (2011). Local strains were detected by measuring the variation in original lengths of the black lines marked on the membrane and the distance in between (**Fig. 10**).

Measured vertical and horizontal local strains during the undrained shearing are shown in **Fig. 11**. Although the trend of the local strain measurements was similar to the total vertical strain measured by the LVDT (Linear Variable Differential Transformer) outside the cell, there were some differences that need to be considered. For example, a good correlation between total strain and AB, BC, and AE local strains was observed. However, CD and BD were smaller and DE was larger than the total vertical strain (**Fig. 11a**). The upper part of the specimen showed a more uniform behavior than the lower part during post-erosion shearing.

In **Fig. 11b**, the horizontal local strains and total vertical strains are compared against one another. It can be seen that the horizontal local strains at B and C were approximately similar in magnitude to the total vertical strains, whereas the lateral strains at A and D were much smaller than those in the middle sections. Furthermore, the lateral deformation in the lower part of the specimen was larger than in the upper part.

Inevitably, there is always friction between the loading ram and triaxial cell. When the LVDT is installed outside the triaxial chamber and the loading ram is not attached to the loading frame

FIG. 10
(a) Initial and (b) deformed specimen during post-erosion monotonic loading.

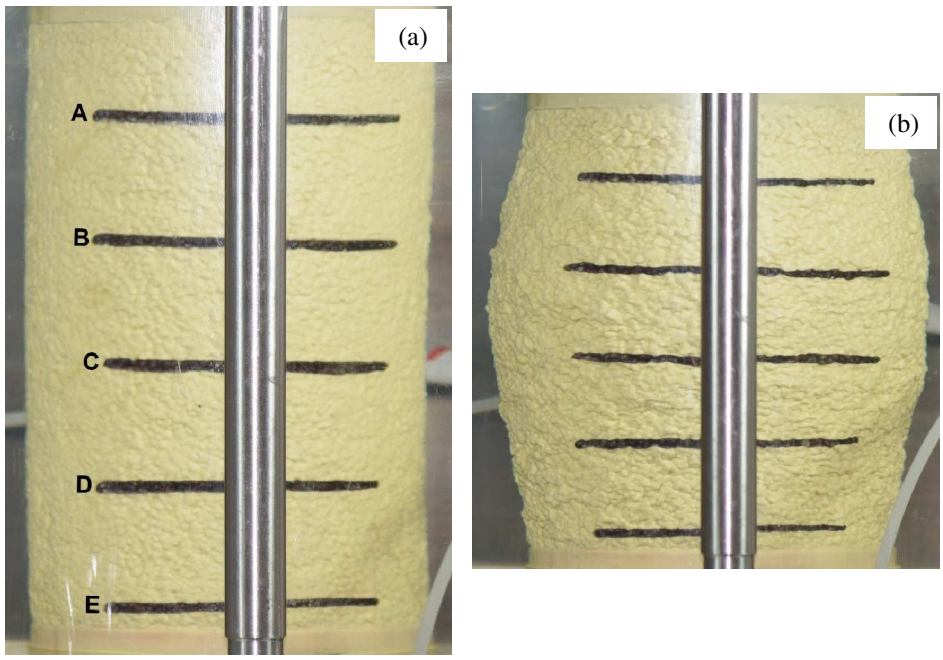

FIG. 11 (a) Local vertical strains and (b) local horizontal strains during monotonic loading.

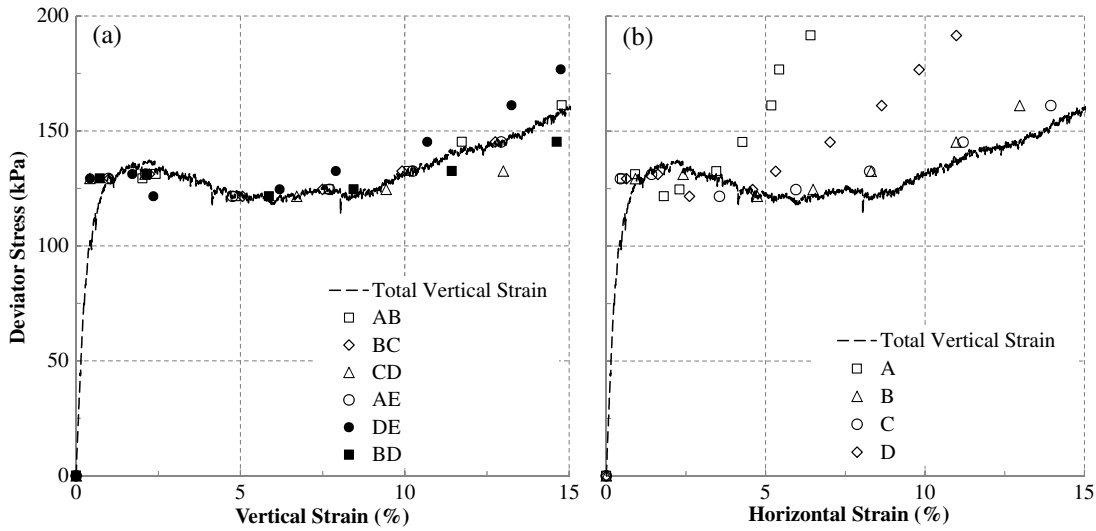

and not locked to the specimen top cap, it is very difficult to consider the friction impact on the deformation measurement. Thus, the LVDT reading is not completely accurate during the erosion stage. Moreover, when the erosion deformation is small, locking the top cap to the load cell may act as a supporting element for the specimen due to the abovementioned friction, which can reduce the erosion deformations, especially for soil samples that show high resistance to erosion. Therefore, locking the top cap is not recommended for the erosion tests unless the post-erosion cyclic behavior needs to be investigated.

Fig. 12 presents the undrained behavior for the soil specimens (pre and post erosion) under cyclic loading followed by undrained monotonic loading (shearing). **Fig. 12a** and **12b** show the cyclic resistance of the soil specimens pre and post erosion. It can be seen that the non-eroded specimen was liquefied in less than five loading cycles, whereas the eroded specimen not only resisted the liquefaction, but the EPWP did not develop considerably (**Fig. 12c**). Thus, **Fig. 12** suggests that losing the fine particles increased the cyclic resistance of the soil remarkably. This is in agreement with what was reported by Ke and Takahashi

FIG. 12 Pre- and post-erosion response under cyclic loading: (a) stress-strain response under cyclic loading and post-cyclic shearing, (b) stress-strain response under cyclic loading, (c) induced EPWP during cyclic loadings and post-cyclic shearing, and (d) stress path during cyclic loading and post-cyclic shearing.

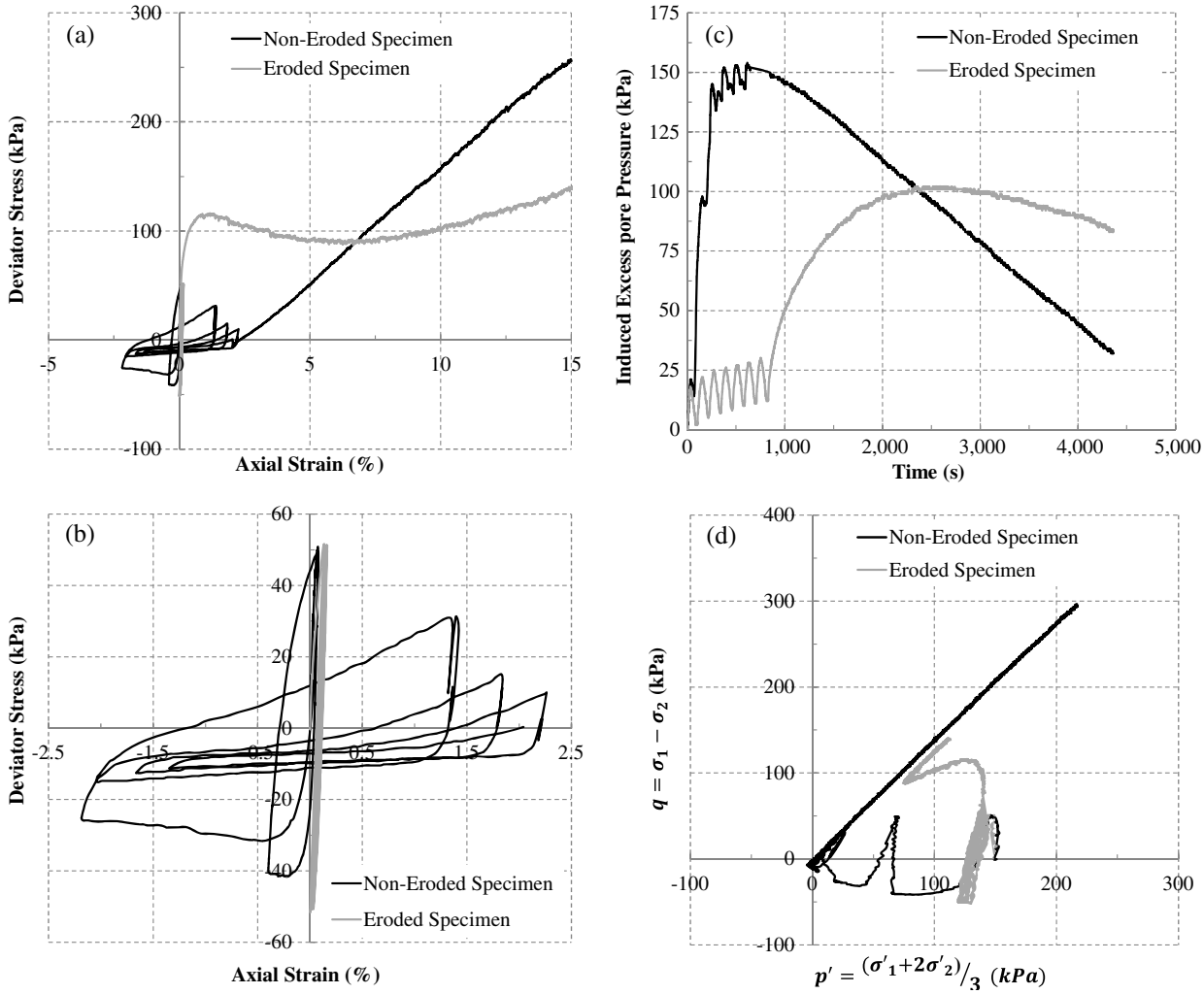

(2014a) that the eroded specimen failed after more cycles of loading.

At first glance this seems to be a contradiction to the static triaxial test results presented in **Fig. 9**, which suggested that the local concentration of fine particles after erosion decreased the shear strength. However, it is important to note that less than 0.2 % vertical strain occurred during cyclic loading. As can be seen from **Fig. 9a**, at the small strains the shear strength of the eroded specimen was greater than the non-eroded specimen.

The stress-strain trend and shear strength results were similar to the results obtained under monotonic loading for the eroded specimens (**Figs. 9a** and **12a**). The development of EPWP was minor for the eroded specimen during cyclic loading in comparison with the non-eroded specimen. In contrast, the non-eroded specimen showed dilation immediately after cyclic loadings, whereas the eroded one contracted and developed a positive EPWP first and dilative behavior wasn't observed until after 6 % axial strain (**Fig. 12c**). The stress paths during and post cyclic loading were completely different as the eroded and non-eroded specimens behaved differently. However, the angle of the steady state lines were similar regardless of the amount of fine particle loss (**Fig. 12d**).

It is also worth mentioning that the soil skeleton stayed stable during the erosion stage. Although 66 % of the fine particles was eroded, no considerable settlement was observed (less than 1 % (**Fig. 8b**). This suggests that even though the erosion of the fine particles changed the behavior of the soil, it did not affect the soil structure at a global scale. In other words, although the fine particles did not contribute to the primary soil matrix and only filled the voids and provided the lateral support, they did play a tangible role during shearing. By performing erosion phase under higher

FIG. 13 Post-erosion particle size distribution of a (a) whole sample and (b) at different levels.

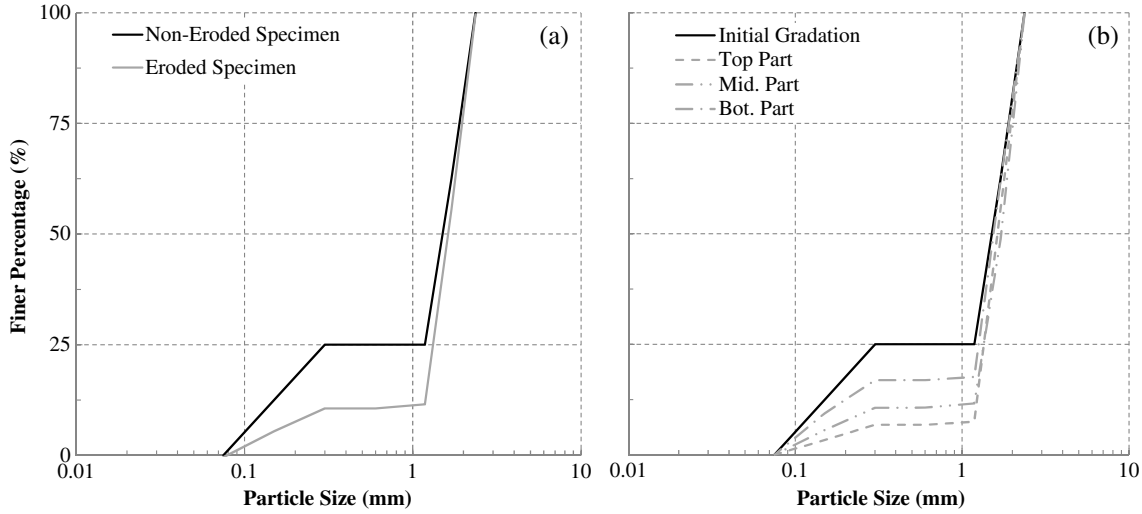

FIG. 14 Repeatability of (a) monotonic shearing: stress-strain behaviour, (b) monotonic shearing: induced excess pore pressure, (c) post-cyclic shearing: stress-strain behaviour and (d) cyclic and post-cyclic shearing: induced excess pore pressure.

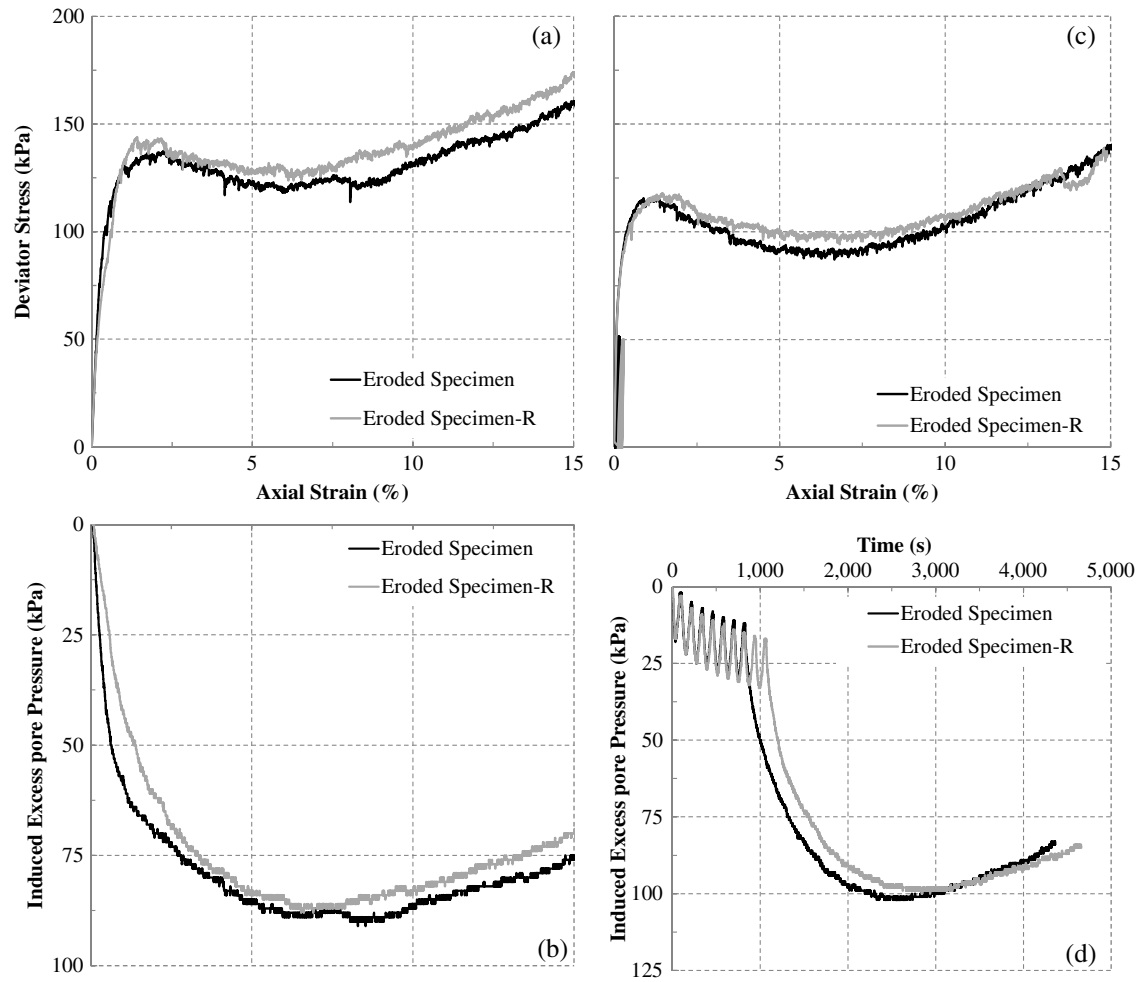

inflows, participation of the survived fine particles in the force chains can be investigated.

PEPSD of an eroded specimen is shown in **Fig. 13**. The flat part of the soil gradation curve moved downward after suffusion as expected (**Fig. 13a**). The erosion of the fine particles was more obvious in the top section of the specimen under downward flow, which is in agreement with Moffat and Fannin (2006), Chang and Zhang (2011), and Ke and Takahashi (2014a) (**Fig. 13b**). Results of the photogrammetry technique showed that the upper region of the eroded specimen experienced a more uniform deformation than the lower region during undrained shearing. However, based on the PEPSDs, the upper part lost more fine particles. It is evident that a considerable percentage of the survived fine particles in the lower part belonged to the upper parts that were clogged downstream. Therefore, the initial uniformity (as provided during sample preparation) was not present anymore. Although the upper region of the specimens lost most of the fine particles, a clean and robust coarse structure remained. However, due to the fine particles spreading non-uniformly across the lower region of the specimen, this led to a different behavior during shearing. This confirmed that the global void ratio is not an accurate index for assessing the post-erosion behaviour.

Repeatability

Repeatability of the post-erosion triaxial test results under monotonic loading and cyclic loading followed by monotonic shearing is shown in **Fig. 14**. Each test was repeated to ensure validity of the results. From this figure, it can be seen that the tests were reasonably consistent for all eroded specimens. The only minor observed deviation could be explained due to the non-uniformity of the reconstituted samples during preparation or the small difference in the final quantity of the eroded particles.

Conclusions

In this study, a versatile apparatus was developed from a conventional triaxial chamber to investigate the post-erosion behavior of granular type soils. This newly developed system is capable of performing erosion inside the triaxial cell on different sized specimens at various stress paths, hydraulic conditions, and loading patterns. The effect of suffusion on the mechanical properties of an internally unstable soil was investigated. The gap-graded soil specimens with 25 % fine content were reconstituted using the moist tamping method and consolidated to 150 kPa to remove the stress history of the specimen during sample preparation. A constant flow rate was applied at the top of the specimens for two hours, whereas the back pressure was kept constant (to maintain full stauration). All specimens then experienced undrained shearing under monotonic or cyclic loading. The following points were the most important findings of this research:

- U.S. Army Corps of Engineers (1953), Istomina (1957), Kwang (1990), and Chang and Zhang (2013) among other criteria mis-anticipated internal stability of the soil mixture used in this research.
- The behavior of the soil tested changed from strain hardening behavior to limited flow deformation after erosion. This change increased the undrained shear strength across the small vertical strain range (i.e., up to 4 %) and improved the soil resistance against cyclic loading. The initial stiffness was similar pre and post erosion. However, the eroded specimen became softer over the medium strain range (i.e., 4–8 %).
- The non-eroded and eroded specimens showed contractive behavior first, followed by dilation. The dilative behavior was more obvious in the non-eroded specimens.
- Although 66 % of the fine particles was eroded during erosion, none of the specimens experienced considerable global vertical deformation (less than 1 % vertical strains). However, the soil behavior changed completely. It showed that although the fine particles may not have contributed to the primary soil fabric, their lubricating effect need to be considered.
- The flow deformation of the eroded specimens across the medium vertical strain range (i.e., 4–8 %) was attributed to the local concentration of fine particles or the larger global void ratio. This effect was later overcome by additional shearing and activation of dilatancy. Moreover, it was understood that erosion of the semi-active fine particles that provided lateral support for the coarse particles led to local particle rearrangements. These particle rearrangements decreased the intergranular void ratio and were recognized in vertical strains where a sudden spike occurred. This finding indicates that the post-erosion behavior cannot be explained only by the global void ratio, and increase in the global void ratio does not necessarily mean that the eroded soil moves to a looser state. Inherent behavior of coarse particles, particle shape, and contribution of fine particles in the soil stress matrix also need to be taken into account. More investigation, particularly x-ray tomography, needs to be conducted to confirm this.

ACKNOWLEDGMENTS

The authors acknowledge the support provided through "Melbourne-Sarawak Research Collaboration Scheme," funded by Swinburne University of Technology, Australia.

References

Ahlinhan, M. F. and Achmus, M., 2010, "Experimental Investigation of Critical Hydraulic Gradients for Unstable Soils," presented at the *5th International Conference on Scour and Erosion*, San Francisco, CA, American Society of Civil Engineers, Reston, VA, pp. 599–608.

Bendahmane, F., Marot, D., and Alexis, A., 2008, "Experimental Parametric Study of Suffusion and Backward Erosion," *J. Geotech. Geoenviron. Eng.*, Vol. 134, No. 1, pp. 57–67.

Bradshaw, A. S. and Baxter, C. D. P., 2007, "Sample Preparation of Silts for Liquefaction Testing," *Geotech. Test. J.*, Vol. 30, No. 4, pp. 324–332.

Burenkova, V. V., 1993, "Assessment of Suffusion in Non-Cohesive and Graded Soils," presented at the *1st International Conference on Geo-Filters*, Balkema, Rotterdam, The Netherlands, pp. 357–360.

Carraro, J. A. and Prezzi, M., 2008, "A New Slurry-Based Method of Preparation of Specimens of Sand Containing Fines," *Geotech. Test. J.*, Vol. 31, No. 1, pp. 1–11.

Chang, D. S. and Zhang, L. M., 2011, "A Stress-Controlled Erosion Apparatus for Studying Internal Erosion in Soils," *Geotech. Test. J.*, Vol. 34, No. 6, pp. 579–589.

Chang, D. S. and Zhang, L. M., 2013, "Extended Internal Stability Criteria for Soils Under Seepage," *Soils Found.*, Vol. 53, No. 4, pp. 569–583.

Dallo, Y. A., Wang, Y., and Ahmed, O. Y., 2013, "Assessment of the Internal Stability of Granular Soils Against Suffusion," *Eur. J. Environ. Civ. Eng.*, Vol. 17, No. 4, pp. 219–230.

Ferreira, T. and Rasband, W., 2012, "ImageJ User Guide," *IJ1. 46r*, Natl. Inst. Health, Bethesda, MD, 2012, https://web.archive.org/web/20170916195530/https://imagej.nih.gov/ij/docs/guide/user-guide.pdf/ (accessed 16 Sept. 2017).

Fleshman, M. S. and Rice, J. D., 2014, "Laboratory Modelling of the Mechanisms of Piping Erosion Initiation," *J. Geotech. Geoenviron. Eng.*, Vol. 140, No. 6, https://doi.org/10.1061/(ASCE)GT.1943-5606.0001106

Fraser, H. J., 1935, "Experimental Study of the Porosity and Permeability of Elastic Sediments," *J. Geol.*, Vol. 43, No. 8, pp. 910–1010.

Frost, J. D. and Park, J. Y., 2003, "A Critical Assessment of the Moist Tamping Technique," *Geotech. Test. J.*, Vol. 26, No. 1, pp. 57–70.

Guimaraes, M., 2002, "Crushed Stone Fines and Ion Removal from Clay Slurries-Fundamental Studies," Dissertation, Georgia Institute of Technology, Atlanta, GA.

Hicher, P. Y., 2013, "Modelling the Impact of Particle Removal on Granular Material Behaviour," *Géotechnique*, Vol. 63, No. 2, pp. 118–128.

Indraratna, B., Israr, J., and Rujikiatkamjorn, C., 2015, "Geometrical Method for Evaluating the Internal Instability of Granular Filters Based on Constriction Size Distribution," *J. Geotech. Geoenviron. Eng.*, Vol. 141, No. 10, pp. 1–14, https://doi.org/10.1061/(ASCE)GT.1943-5606.0001343

Indraratna, B., Raut, A. K., and Khabbaz, H., 2007, "Constriction-Based Retention Criterion for Granular Filter Design," *J. Geotech. Geoenviron. Eng.*, Vol. 133, No. 3, pp. 266–276.

International Commission on Large Dams (ICOLD), 2015, "Internal Erosion of Existing Dams, Levees and Dikes, and Their Foundations," Bulletin 164, Paris.

Ishihara, K., 1993, "Liquefaction and Flow Failure During Earthquakes," *Géotechnique*, Vol. 43, No. 3, pp. 351–451.

Istomina, V. S., 1957, "Filtration Stability of Soils," Gostroizdat, Moscow.

Jiang, M. J., Konrad, J. M., and Leroueil, S., 2003, "An Efficient Technique for Generating Homogeneous Specimens for DEM Studies," *Comput. Geotech.*, Vol. 30, No. 7, pp. 579–597.

Ke, L. and Takahashi, A., 2012, "Strength Reduction of Cohesionless Soil Due to Internal Erosion Induced by One-Dimensional Upward Seepage Flow," *Soils Found.*, Vol. 52, No. 4, pp. 698–711.

Ke, L. and Takahashi, A., 2014a, "Triaxial Erosion Test for Evaluation of Mechanical Consequences of Internal Erosion," *Geotech. Test. J.*, Vol. 37, No. 2, pp. 1–18.

Ke, L. and Takahashi, A., 2014b, "Experimental Investigations on Suffusion Characteristics and its Mechanical Consequences on Saturated Cohesionless Soil," *Soils Found.*, Vol. 54, No. 4, pp. 713–730.

Ke, L. and Takahashi, A., 2015, "Drained Monotonic Responses of Suffusional Cohesionless Soils," *J. Geotech. Geoenviron. Eng.*, Vol. 141, No. 8, https://doi.org/10.1061/(ASCE)GT.1943-5606.0001327, 04015033

Kenney, T. C., Chahal, R., Chiu, E., Ofoegbu, G. I., Omange, G. N., and Ume, C. A., 1985, "Controlling Constriction Sizes of Granular Filters," *Can. Geotech. J.*, Vol. 22, No. 1, pp. 32–43.

Kenney, T. C. and Lau, D., 1985, "Internal Stability of Granular Filters," *Can. Geotech. J.*, Vol. 22, No. 2, pp. 215–225, https://doi.org/10.1139/t85-029

Kenney, T. C. and Lau, D., 1986, "Internal Stability of Granular Filters: Reply," *Can. Geotech. J.*, Vol. 23, No. 4, pp. 420–423, https://doi.org/10.1139/t86-068

Kezdi, A., 1969, "Increase of Protective Capacity of Flood Control Dikes," Budapest University of Technology and Economics, Budapest. Report No. 1. (in Hungarian).

Kuerbis, R. and Vaid, Y. P., 1988, "Sand Sample Preparation-The Slurry Deposition Method," *Soils Found.*, Vol. 28, No. 4, pp. 107–118.

Kwang, T., 1990, "Improvement of Dam Filter Criterion for Cohesionless Base Soil," M. Eng. thesis, Asian Institute of Technology, Bangkok, Thailand.

Ladd, R. S., 1978, "Preparing Test Specimens Using Undercompaction," *Geotech. Test. J.*, Vol. 1, No. 1, pp. 16–23.

Li, M. and Fannin, R. J., 2011, "A Theoretical Envelope for Internal Instability of Cohesionless Soil," *Géotechnique*, Vol. 62, No. 1, pp. 77–80.

Luo, Y. L., Qiao, L., Liu, X. X., Zhan, M. L., and Sheng, J. C., 2013, "Hydro-Mechanical Experiments on Suffusion Under Long-Term Large Hydraulic Heads," *Nat. Hazards*, Vol. 65, No. 3, pp. 1361–1377.

Mao, C. X., 2005, "Study on Piping and Filters. Part 1: Piping (in Chinese)," *Rock Soil Mech.*, Vol. 26, No. 2, pp. 209–215.

Marot, D., Bendahmane, F., and Nguyen, H. H., 2012, "Influence of Angularity of Coarse Fraction Grains on Internal Erosion Process," *La Houille Blanche*, Vol. 6, pp. 47–53.

Mehdizadeh, A., Disfani, M. M., Evans, R. P., Arulrajah, A., and Ong, D. E. L., 2015, "Discussion of 'Development of an Internal Camera-Based Volume Determination System for Triaxial Testing' by S. E. Salazar, A. Barnes, and R. A. Coffman," *Geotech. Test. J.*, Vol. 38, No. 1, pp. 165–168, https://doi.org/10.1520/GTJ20150153

Mitchell, J. K., 1993, *Fundamentals of Soil Behavior*, John Wiley & Sons, Inc., New York, N. Y., pp. 1–210.

Moffat, R. A. and Fannin, R. J., 2006, "A Large Permeameter for Study of Internal Stability in Cohesionless Soils," *Geotech. Test. J.*, Vol. 29, No. 4, pp. 273–279.

Moffat, R. and Fannin, R. J, 2011, "A Hydromechanical Relation Governing Internal Stability of Cohesionless Soil," *Can. Geotech. J.*, Vol. 48, No. 3, pp. 413–424.

Moffat, R., Fannin, R. J., and Garner, S. J, 2011, "Spatial and Temporal Progression of Internal Erosion in Cohesionless Soil," *Can. Geotech. J.*, Vol. 48, No. 3, pp. 399–412.

Moffat, R. and Herrera, P., 2014, "Hydromechanical Model for Internal Erosion and Its Relationship with the Stress Transmitted by the Finer Soil Fraction," *Acta Geotech.*, Vol. 10, No. 5, pp. 643–650.

Moraci, N., Mandaglio, M. C., and Ielo, D., 2014, "Analysis of the Internal Stability of Granular Soils Using Different Methods," *Can. Geotech. J.*, Vol. 51, No. 9, pp. 1063–1072.

Ouyang, M. and Takahashi, A., 2015, "Influence of Initial Fines Content on Fabric of Soils Subjected to Internal Erosion," *Can. Geotech. J.*, Vol. 53, No. 2, pp. 299–313.

Richards, K. S. and Reddy, K. R., 2008, "Experimental Investigation of Piping Potential in Earthen Structures," *Geotech. Special Pub.*, No. 178, pp. 367–376.

Sail, Y., Marot, D., Sibille, L., and Alexis, A., 2011, "Suffusion Tests on Cohesionless Granular Matter: Experimental Study," *Eur. J. Environ. Civ. Eng.*, Vol. 15, No. 5, pp. 799–817.

Shire, T., O'Sullivan, C., Hanley, K. J., and Fannin, R. J., 2014, "Fabric and Effective Stress Distribution in Internally Unstable Soils," *J. Geotech. Geoenviron. Eng.*, Vol. 140, No. 12.

Scholtès, L., Hicher, P. Y., and Sibille, L., 2010, "Multiscale approaches to describe mechanical responses induced by particle removal in granular materials," *Comptes Rendus Mécanique*, Vol. 338, No. 10, pp. 627–638.

Sherard, J. L., 1979, "Sinkholes in Dams of Coarse, Broadly Graded Soils," in transactions of the *13th International Congress on Large Dams*, New Delhi, India, International Commission on Large Dams, Paris, pp. 25–34.

Skempton, A. W. and Brogan, J. M., 1994, "Experiments on Piping in Sandy Gravels," *Géotechnique*, Vol. 44, No. 3, pp. 449–460.

Terzaghi, K., 1925, "Erdbaumechanik auf bodensphysikalischer grundlage," *Franz Deuticke*, Vienna.

Uchaipichat, A., Khalili, N., and Zargarbashi, S., 2011, "A Temperature Controlled Triaxial Apparatus for Testing Unsaturated Soils," *Geotech. Test. J.*, Vol. 34, No. 5, pp. 424–432.

U.S. Army Corps of Engineers, 1953, "Filter Experiments and Design Criteria," Waterways Experiment Station, Vicksburg, MS, Technical Memorandum No. 3–360.

Wood, D. M., Maeda, K., and Nukudani, E., 2010, "Modelling Mechanical Consequences of Erosion," *Géotechnique*, Vol. 60, No. 6, pp. 447–457.

Xiao, M. and Shwiyhat, N., 2012, "Experimental Investigation of the Effects of Suffusion on Physical and Geomechanic Characteristics of Sandy Soils," *Geotech. Test. J.*, Vol. 35, No. 6, pp. 890–900.